Urban Climate 46 (2022) 101346

Contents lists available at ScienceDirect

Urban Climate

journal homepage: www.elsevier.com/locate/uclim

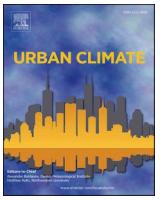

An analytical approximation of urban heat and dry islands and their impact on convection triggering

Clinton T.F. Chiu [a], Kai Wang [a,f], Athanasios Paschalis [b], Tohid Erfani [a], Nadav Peleg [c], Simone Fatichi [d], Natalie Theeuwes [e], Gabriele Manoli [a,g,*]

[a] Department of Civil, Environmental, and Geomatic Engineering, University College London, UK
[b] Department of Civil and Environmental Engineering, Imperial College London, UK
[c] Institute of Earth Surface Dynamics, University of Lausanne, Switzerland
[d] Department of Civil and Environmental Engineering, National University of Singapore, Singapore
[e] Royal Netherlands Meteorological Institute, the Netherlands
[f] China-UK Low Carbon College, Shanghai Jiao Tong University, Shanghai, China
[g] School of Architecture, Civil and Environmental Engineering, École Polytechnique Fédérale de Lausanne (EPFL), Lausanne, Switzerland

ARTICLE INFO

Keywords:
Urban Heat Island
Urban Dry Island
Boundary layer
Convective clouds
Analytical model

ABSTRACT

It is well known that cities increase air and surface temperatures compared to their rural surroundings, the so-called urban heat island (UHI) effect. However, the associated changes in atmospheric humidity (also known as urban dry island, UDI) and convection triggering remain largely unexplored and it is still unclear how urban modifications of the surface energy budget influence the diurnal evolution of temperature and humidity in the Atmospheric Boundary Layer (ABL) and ultimately control the initiation of convective clouds.

Here we quantify the impact of different urban settings and free atmospheric conditions on UHI, UDI, and convection triggers by means of a zero-order model of the ABL. Specifically, we derive an approximate solution for urban-rural changes in surface energy fluxes and ABL potential temperature and humidity and we investigate the crossing between the ABL height and the lifting condensation level (LCL) which is a proxy for the triggering of convective clouds. We show that urban areas are generally warmer and drier, thus causing an increase in both ABL and LCL heights. However, the response of the ABL-LCL crossing to surface conditions is non-linear and there exists a range of free atmosphere conditions for which changes in imperviousness can impact convective clouds.

1. Introduction

By the year 2050, it is estimated that 68% of the world's population will live in cities (UN-DESA, 2018). Human activity in urban environments causes changes in the atmospheric composition, altering the the surface and atmospheric conditions, and has significant impacts on urban warming (e.g. Shepherd, 2005; Grimmond, 2007; Pataki et al., 2011; Grimmond et al., 2015). Moreover, urbanisation leads to large scale land-cover changes that strongly influence the energy balance at the land surface, with implications for both local and regional climate (Oke et al., 2017). One of the most studied impacts of cities on the atmospheric environment is the urban

* Corresponding author.
E-mail address: gabriele.manoli@epfl.ch (G. Manoli).

https://doi.org/10.1016/j.uclim.2022.101346
Received 22 December 2021; Received in revised form 1 July 2022; Accepted 5 November 2022

heat island (UHI) effect (e.g. Howard, 1833; Oke, 1973; Manoli et al., 2019). In urban areas, the natural land cover is replaced by impervious surfaces and buildings that modify surface roughness and albedo, as well as storage of heat and evapotranspiration fluxes, leading to an increase in surface temperatures during daytime and causing higher air temperatures during the evening and into the night compared to the rural surroundings (e.g. Oke, 1982; Arnfield, 2005; Bouyer, 2009; Theeuwes et al., 2017; Manoli et al., 2020a; Paschalis et al., 2021; Venter et al., 2021; Zhang et al., 2022).

The reduction in evapotranspiration fluxes associated with the imperviousness of urban areas has been shown to be a major control of urban warming, both in terms of surface and canopy urban heat islands (SUHI and CUHI, respectively) (e.g. Li et al., 2019; Du et al., 2021; Venter et al., 2021). However, the correlation between SUHI and CUHI on short (e.g. daily) timescales remain a subject of debate (e.g. Martilli et al., 2020; Manoli et al., 2020b) due to the complex relationship between air and surface temperatures.

The reduction in evaporative cooling also acts to decrease atmospheric humidity and increase vapor pressure deficits, a phenomenon called the Urban Dry Island (UDI) effect (e.g. Hao et al., 2018). Yet, recent studies suggest that cities can enhance - rather than suppress - convective cloud formation (Theeuwes et al., 2019) because, despite lower humidity, heat release from built surfaces can influence atmospheric boundary layer dynamics and initiate summertime convection, potentially intensifying thunderstorms and extreme rainfall (e.g. Risser and Wehner, 2017; Zhang et al., 2018; Huang et al., 2022). Observations by Theeuwes et al. (2019) showed a systematic enhancement of summertime and late spring cloud cover in the afternoon and evening hours over the two large metropolitan areas of Paris and London. Long-term measurements located in and around London showed that low clouds can persist longer over the urban area than in the rural surroundings even if less moisture is available at the surface and the atmosphere is drier because surface heating is higher. However, according to Zhu et al. (2017), such enhanced convection over cities is attributable to moisture advection from the surrounding rural areas rather than the UHI effect.

How urban areas influence energy and water budgets and ultimately alter cloud formation mechanisms thus remains a subject of research as convection triggering depends on the interplay between surface and free atmosphere conditions and the resulting diurnal evolution of temperature and humidity in the atmospheric boundary layer (ABL) (e.g. Pielke, 2001; Garcia-Carreras et al., 2011; Manoli et al., 2019). Here we focus on daytime UHIs and convective boundary-layer clouds as they are directly impacted by latent and sensible heat fluxes at the land surface (e.g. Betts et al., 1996; Ek and Holtslag, 2004)). Such convective clouds typically occur during summertime because radiation and thus sensible heat is much larger in summer than in winter. Winter conditions are not as likely to

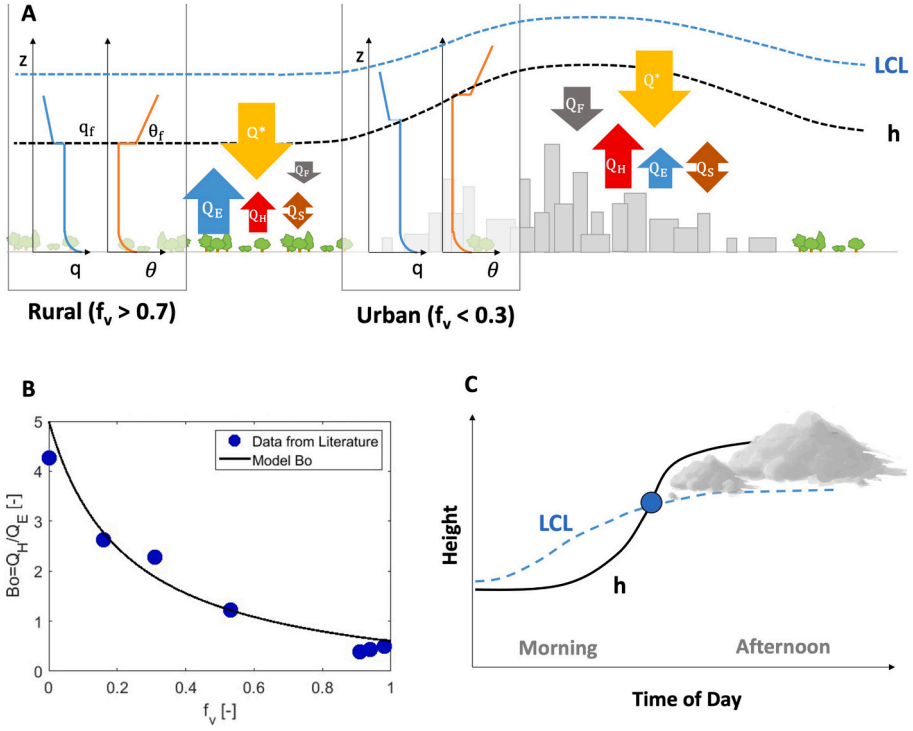

Fig. 1. (A) Schematic representation of the conceptual slab ABL model: the left part represents the rural fluxes, including net radiation Q^*(yellow downward arrow), sensible heat flux H (red upward arrow), latent heat flux LE (blue upward arrow) and storage heat flux ΔQ_S (brown downward arrow). On the right, the graph represents the urban fluxes. Lifting Condensation Level height (blue dotted lines) and Atmospheric Boundary Layer height (black dotted lines) are also shown, the vertical profile of specific humidity q and potential temperature θ over rural and urban areas; (B) Bowen Ratio as a function of the vegetation fraction (f_v) of the city: Observed (blue points, retrieved from Christen and Vogt (2004)) and modelled (black line) Bowen Ratio as a function of vegetation fraction f_v; (C) the diurnal crossing of LCL and ABL as a proxy for cloud formation: the blue circle represents the intersection of LCL and ABL when cloud starts to form. (For interpretation of the references to colour in this figure legend, the reader is referred to the web version of this article.)

trigger convection partly due to reduced transpiration rates and evaporative fraction (i.e. higher Bowen Ratio and the lack of buoyancy) (Manoli et al., 2016).

Under clear-sky conditions (hereinafter referred to as fair-weather conditions), convection triggering can be modelled by considering the diurnal evolution of the Atmospheric Boundary Layer (ABL) and its first crossing with the Lifting Condensation Level (LCL), which represents the thermodynamic condition for saturation of air parcels and can be recognised as the cloud base height (e.g. Siqueira et al., 2009). This crossing is a necessary condition for the formation of simple cumuli and shallow stratocumuli (Stevens, 2006), and offers a simple metric for exploring how changes in surface conditions can impact the persistence and transition of the atmospheric system between cloudy and cloudless regimes (e.g. Juang et al., 2007; Siqueira et al., 2009; Konings et al., 2010; Bonetti et al., 2015; Manoli et al., 2016). Many studies investigated how changes in soil moisture and evapotranspiration alter the diurnal evolution of the ABL and the likelihood of convection over natural surfaces (e.g. Findell and Eltahir, 2003; Gentine et al., 2013b; Yin et al., 2015; Bhowmick and Parker, 2018). It was found that cumulus onset is favored in the case of low Bowen ratio (i.e. wet soil) and moderate to high stability, while in less stable environments, convection is favored in high Bowen ratio (i.e. dry soil) regimes (Haiden, 1997). Further studies confirmed that the triggering of convective clouds depends on the Bowen ratio and the stability above the ABL, with the sensitivity to surface conditions (i.e. dry vs wet soil) varying with the stability of the vertical profile (e.g. Ek and Mahrt, 1994; Findell and Eltahir, 2003; Bhowmick and Parker, 2018). The impervious surfaces of cities result in Bowen ratio values that are comparable with dry soil conditions (Fig. 1), potentially leading to similar changes in the diurnal evolution of the ABL and the onset of convective clouds. However, such dynamics remain largely unexplored in urban settings (e.g. Romanov, 1999; Angevine et al., 2003; Theeuwes et al., 2019).

The main objective of this study is thus to (i) model the intensity of the UHI and UDI effects across different urban-rural gradients and free atmosphere conditions and (ii) identify their potential impacts on the initiation of convective clouds. Specifically, we present a parsimonious description of the ABL diurnal evolution and associated temperature and humidity budgets and derive an analytical solution for urban-rural changes in temperature, humidity, and the timing and occurrence of the ABL-LCL crossing. The presented framework allows to quantify the impact of urban imperviousness on boundary layer dynamics, thus disentangling the relative effect of surface and free atmosphere conditions on urban warming, drying, and convection triggering.

2. Methodology

2.1. Model development

To describe land-atmosphere interactions over different land use scenarios, we present a zeroth-order model that couples a surface energy balance with a slab representation of the ABL, employing different parameterisations to distinguish between urban and rural surfaces (Fig. 1A). Specifically, the available net radiation Q^* is partitioned into sensible (Q_H) and latent (Q_E) heat fluxes, depending on the Bowen Ratio ($Bo = Q_H/Q_E$) of each surface.

Boundary layer dynamics are described by the ABL height (h), potential temperature (θ) and specific humidity (q) in the well-mixed ABL, and the height of the Lifting Condensation Level (LCL). For the Free Atmosphere (FA), we assume vertical linear profiles of θ and q and describe the FA state; which depends on synoptic scale dynamics - considering the temperature and humidity lapse rates γ_θ and γ_q, respectively (e.g. Porporato, 2009; Gentine et al., 2013a; Manoli et al., 2016). In this framework, the diurnal evolution of the ABL responds to both surface energy fluxes and entrainment at the ABL top (Driedonks et al., 1984), and the formation of convective clouds can be described, as a first order approximation, by the crossing of the ABL height with the LCL (e.g. Betts et al., 1996; Betts, 2009; Manoli et al., 2016).

Given the aim of deriving an analytical solution for urban-rural changes in ABL dynamics, the following assumptions are made: (1) urban and rural surfaces are considered large and homogeneous enough to assume a well-mixed ABL; (2) only vertical exchange is explicitly modelled, while regional-scale convergence/divergence of heat and moisture (i.e. horizontal advection) are not considered; (3) atmospheric subsidence is neglected; (4) the aerosols impact on cloud formation, precipitation and the heating distribution in the boundary layer are also not explicitly considered; and (5) the Bowen Ratio is assumed to vary with the level of imperviousness of the surface but it is constant throughout the day. In short, we represent a city as a single column with appropriate thermal characteristics (Fortuniak et al., 2005), we assume that urban surfaces (e.g. buildings, roads) have a common temperature, and we treat urban heterogeneities (e.g. building heights, coverage ratio) implicitly in the surface layer (Kusaka et al., 2001). This has the advantage of simplicity and analytical tractability, reduced computational time and low parameter requirements (Grimmond et al., 2010). Note that the objective here is not to provide a detailed parameterisation to be used in weather/climate models. Rather, we aim to develop a simple toy model to study urban-rural land-atmosphere processes and their sensitivities to changes in surface and FA conditions. Despite its simplifications, this approach can give direction to future observational and modeling studies. In general, the assumption of a constant Bowen Ratio during daytime is in line with observations at the study site (see Supplementary Information, SI) and other cities around the world (Oke et al., 2017), and the use of a slab model of the urban ABL is supported by previous modeling applications (e.g. Onomura et al., 2015). Such a simplified approach is consistent with our focus on large inland cities with flat topography (to remove orographic effects) and with the objective of isolating surface and FA controls (e.g. Bhowmick and Parker, 2018). We also neglect the impact of horizontal circulation on ABL growth and convection, which may be an important factor for many urban areas around the world (Pal et al., 2021). In these regards, we present additional analyses in the discussion section and the SI to account for lateral advection of moisture and heat, and assess their impact on ABL-LCL dynamics. Yet, given the simplified approach presented here and the objective of disentangling the relative importance of surface versus free atmosphere conditions on urban warming/drying, a detailed quantification of advection effects is considered beyond the scope of this study and is left for future work.

2.1.1. Surface energy balance

The surface energy balance (SEB) of urban and rural surfaces can be written as:

$$Q^* + Q_F = Q_H + Q_E + \Delta Q_S + \Delta Q_A, \tag{1}$$

where Q^* is net all-wave radiation [W m^{-2}], assumed to be independent of ABL conditions (Porporato, 2009), Q_F is the anthropogenic heat flux [W m^{-2}] (negligible for rural areas), Q_H is the sensible heat flux [W m^{-2}], Q_E is the latent heat flux [W m^{-2}], ΔQ_S is the net storage heat flux [W m^{-2}], and ΔQ_A is the net heat flux by advection [W m^{-2}].

Here we assume that $\Delta Q_A = 0$ [W m^{-2}]. However, given the potential impact of horizontal advection due to temperature difference between urban and rural areas, a sensitivity analysis to the value of ΔQ_A is provided in the SI. We now introduce the Bowen Ratio $Bo = \frac{Q_H}{Q_E}$, so that we can write the latent heat flux as $Q_E = \frac{Q_H}{Bo}$ and the sensible heat flux as:

$$Q_H = \frac{Bo}{Bo+1}(Q^* + Q_F - \Delta Q_S - \Delta Q_A) \tag{2}$$

The storage heat flux ΔQ_S is estimated from Q^* using the Objective Hysteresis Model (OHM) proposed by Grimmond et al. (1991) as:

$$\Delta Q_S = \sum_i f_i \left[a_{1,i} Q^* + a_{2,i} \frac{dQ^*}{dt} + a_{3,i} \right], \tag{3}$$

where t is the time of the day and f_i is the surface cover fraction of land type i. For the sake of simplicity, we partition the land cover into vegetated (v) and built (b) surfaces only so that $f_v + f_b = 1$ for both urban and rural areas. The OHM Coefficients a_1 [−], a_2 [hour], a_3 [W m^{-2}] are selected from the literature for different surface types (Ward et al., 2016). The parameter a_1 indicates the overall strength of the dependence of the storage heat flux on net radiation, the parameter a_2 is the degree and direction of the phase relations between ΔQ_s and Q^* and the parameter a_3 is an intercept term that indicates the relative timing when ΔQ_s and Q^* turn negative (Grimmond and Oke, 1999). The values of a_1, a_2, a_3 are listed in Table 1. Considering this simplification, Eq. 3 can be rewritten as:

$$\Delta Q_S = A_1 Q^* + A_2 \frac{dQ^*}{dt} + A_3, \tag{4}$$

where $A_1 = f_v \cdot a_{1,\,v} + f_b \cdot a_{1,\,b}$ [−], $A_2 = f_v \cdot a_{2,\,v} \cdot 3600 + f_b \cdot a_{2,\,b} \cdot 3600$ [s], and $A_3 = f_v \cdot a_{3,\,v} + f_b \cdot a_{3,\,b}$ [W m^{-2}].

2.1.2. Atmospheric boundary layer dynamics

The diurnal evolution of the ABL height (h [m]) is described by the following ordinary differential equation (e.g. Tennekes, 1973; Garratt, 1993; Porporato, 2009):

$$\frac{dh}{dt} = \frac{(1+2\beta)Q_H}{\rho c_p \gamma_\theta h}, \tag{5}$$

Table 1
List of parameters used for urban and rural simulations.

Description	Parameters	Urban	Rural	Unit
Daily maximum net radiation	Q_m	660	600	W m^{-2}
Day Length	t	11.6	11.6	hour
Time of Sunrise	t_0	5.8	5.8	hour
Advection Heat Flux	ΔQ_A	0	0	W m^{-2}
Anthropogenic Heat Flux	Q_F	20	0	W m^{-2}
Bowen Ratio	Bo	2.47	0.6	–
Vegetation Fraction	f_v	0.2	0.98	–
Entrainment Efficiency	β	0.2	0.2	–
Potential Temperature Lapse Rate	γ_θ	0.0078	0.0078	K m^{-1}
Specific Humidity Lapse Rate	γ_q	-1×10^{-6}	-1×10^{-6}	kg kg^{-1} m^{-1}
OHM Coefficient	$a1$	0.477	0.215	–
OHM Coefficient	$a2$	0.337	0.1	h
OHM Coefficient	$a3$	−33.9	−19.9	W m^{-2}
Mean Building Height	z_h	12.5	3	m
Aerodynamic Resistance	r_{ah}	53	66	s m^{-1}
Boundary Layer Conductance to sensible heat	g_h	0.02	0.0152	m s^{-1}
Boundary Layer Conductance to latent heat	g_e	0.02	0.0152	m s^{-1}
Initial Boundary Layer Height	h_0	420	100	m
Global Parameter	k_{Bo}	0.2	0.2	–
Initial Mixed-Layer Potential temperature	θ_{f0}	288	288	K
Initial Mixed-Layer Specific humidity	q_{f0}	0.00785	0.00785	kg kg^{-1}

where β is the entrainment efficiency, here assumed to be 0.2 (i.e. the fraction of sensible heat flux from the entrainment at the top of the ABL (Tennekes, 1973)), ρ is the air density assumed constant for simplicity, 1.29 [kg m^{-3}], and c_p=1005 [J kg^{-1} K^{-1}] is the specific heat capacity of air at constant pressure.

The diurnal evolution of potential temperature and specific humidity in the ABL is governed by the conservation equations for heat and moisture in the well-mixed ABL, which are written as (Porporato, 2009):

$$\rho c_p h \frac{d\theta}{dt} = Q_H + \rho c_p (\theta_f - \theta) \frac{dh}{dt}, \tag{6}$$

$$\rho h \frac{dq}{dt} = \frac{Q_E}{\lambda} + \rho (q_f - q) \frac{dh}{dt}, \tag{7}$$

where θ and q are the average boundary layer potential temperature and specific humidity, respectively, $\lambda = 2.45 \times 10^{-6}$ [J kg^{-1}] is the latent heat of vaporisation, θ_f is the potential temperature of the free atmosphere at height $z = h$, and q_f is the specific humidity of the free atmosphere at height $z = h$. Potential temperature and specific humidity in the FA are assumed to follow a linear profile (Porporato, 2009), so that:

$$\theta_f = \gamma_\theta z + \theta_{f0}, \tag{8}$$

$$q_f = \gamma_q z + q_{f0}, \tag{9}$$

where γ_θ and γ_q are, respectively, the potential temperature [K m^{-1}] and specific humidity lapse rates [kg kg^{-1} m^{-1}] of the free atmosphere (see Table 1), θ_{f0} and q_{f0} are the intercept of the vertical linear profiles (see Table 1).

2.1.3. Analytical solution

In this section we present an analytical solution of Eq. 1–8 valid for daytime conditions only. Following Porporato (2009), we approximate the diurnal evolution of net radiation with a parabolic function, that is:

$$Q^*(t) = Q_m \left[1 - \left(\frac{t}{t_0} - 1 \right)^2 \right], \tag{10}$$

where Q_m is the daily maximum net radiation [W m^{-2}] and $0 < t < 2t_0$ is the time of day, $t = 0$ being the time of sunrise, $t = 2t_0$ being day length, and t_0 being the time of maximum radiation (i.e. mid-day). It should be noted that the definition of $0 < t < 2t_0$ is valid for all equations.

Using Eq. 4 and 10, the analytical solution for ΔQ_S can be written as:

$$\Delta Q_S(t) = A_1 Q_m \left[1 - \left(\frac{t}{t_0} - 1 \right)^2 \right] - 2A_2 Q_m \frac{t - t_0}{t_0^2} + A_3, \tag{11}$$

Combining Eq.2,10 and 11, it is now possible to integrate Eq.5 and derive an analytical solution for the diurnal evolution of the ABL height:

$$h(t) = \frac{1}{t_0} \left[\left(h_0^2 t_0^2 + \frac{2}{3} \frac{(1 + 2\beta) Bo \cdot t \left(Q_m t (A_1 - 1)(t - 3t_0) + 3A_2 Q_m (t - 2t_0) + 3t_0^2 (Q_F - A_3) \right)}{\rho c_p \gamma_\theta (Bo + 1)} \right) \right]^{\frac{1}{2}} \tag{12}$$

where h_0 [m] is the ABL height at t=0. To describe the time evolution of potential temperature θ [K] and specific humidity q [kg kg^{-1}] as a function of $h(t)$, we can then employ the solution of Eq.6–30 provided by Porporato (2009), i.e.:

$$\theta(t) = \gamma_\theta \frac{1 + \beta}{1 + 2\beta} h(t) + \theta_{f0}, \tag{13}$$

$$q(t) = \gamma_q^{'} h(t) + q_{f0}, \tag{14}$$

where $\gamma_q^{'}$ is the lapse rate for humidity at the top of the mixed layer, which is defined as:

$$\gamma_q^{'} = \frac{1}{2} \left[\gamma_\theta \frac{c_p}{\lambda (1 + 2\beta) Bo} + \gamma_q \right]. \tag{15}$$

The first term in Eq.31 represents the contribution from the surface evaporation and the second term is from the entrainment from the FA.

2.1.4. Urban heat and Dry Island effects

The analytical solutions derived in the previous section can be applied to urban and rural areas and used to quantify the UHI and UDI effects. An urban heat island occurs when the urban area experiences warmer temperature than its nearby rural area and three

main types of UHI have been identified (Oke et al., 2017): Boundary Layer Urban Heat Island (BUHI), Canopy Layer Urban Heat Island (CUHI) and Surface Urban Heat Island (SUHI).

The BUHI can be estimated using Eq.13, i.e. $\Delta\theta(t) = \theta_u(t) - \theta_r(t)$, where θ is the boundary layer average temperature and the subscripts u and r indicate urban and rural areas, respectively. To estimate the SUHI, we estimate surface temperature as (Porporato, 2009):

$$\theta_s(t) = \frac{Q_H r_{ah}}{\rho c_p} + \theta(t), \tag{16}$$

and calculated urban-rural surface temperature differences as $\Delta\theta_s(t) = \theta_{s,\,u}(t) - \theta_{s,\,r}(t)$. Given that the urban canopy layer (UCL) is the layer between the urban surface and the roof level, we estimate the CUHI by calculating urban-rural temperature differences at 2 m height, i.e. $\Delta\theta_{2m}(t) = \theta_{2m,\,u}(t) - \theta_{2m,\,r}(t)$. Air temperature at 2 m is estimated following Theeuwes et al. (2015), i.e.

$$\theta_{2m}(t) = \frac{Q_{H,2m} r_{ah}}{\rho c_p} + \theta(t), \tag{17}$$

where $Q_{H,\,2m} = Q_H(z^*)e^{-k}$ is the sensible heat flux at 2 m height, $Q_H(z^*)$ [W m^{-2}] is the sensible heat flux above the effective building height (calculated using Eq. 2 (Theeuwes et al., 2015)), $k = \frac{c_h(z_e-2)}{z_e}$, c_h is an empirical constant assumed equal to 1.4 (Christen, 2005), and z_e [m] is the effective building height, which is estimated to be 1.2 times the mean building height (z_h).

Similarly, to simulate the UDI effect, we calculate relative humidity differences ΔRH [%] between the urban and rural area, i.e. $\Delta RH(t) = RH_u(t) - RH_r(t)$. Relative humidity is calculated both in the well-mixed boundary layer (RH) and at the evaporating surface (RH_s). Relative humidity in the ABL is given by $RH = 100^*\left(\frac{q}{q_{sat}(\theta)}\right)$ where q [kg kg^{-1}] is the specific humidity in the mixed layer, q_{sat} is the saturation specific humidity [kg kg^{-1}], expressed as $q_{sat} = 0.622\frac{e_{sat}(\theta)}{P-0.378e_{sat}(\theta)}$, and $e_{sat}(\theta)$ [kPa] is the saturation vapor pressure at temperature θ given by the Clausius-Clapeyron relation. Relative humidity at the evaporating surface (RH_s) is given by $RH_s = 100^*\left(\frac{q_s}{q_{sat}(\theta_s)}\right)$ where the saturated specific humidity at the evaporating surface (q_s) is expressed as (Porporato, 2009):

$$q_s(t) = \frac{E \cdot r_{ah}}{\rho} + q, \tag{18}$$

where E is the evaporative flux $\left(E = \frac{Q_E}{\lambda}\right)$ [kg s^{-1}m^{-2}]. Note that the UDI effect can also be estimated using differences in specific - rather than relative - humidity. This is a more direct measure of urban-rural changes in humidity as RH depends also on temperature (Meili et al., 2022). Here we compare model simulations with field observations of RH and illustrate the difference between the diurnal cycles of relative and specific UDIs in the SI.

The analytical description presented in Eq. 13, 14 and 16, also allow to derive a relation between SUHI and BUHI intensities as well as between the BUHI and UDI effects. Specifically, using Eq. 16, the BUHI can be written as:

$$\Delta\theta(t) = \Delta\theta_s(t) - \frac{\Delta C(t)}{\rho c_p}, \tag{19}$$

where $\Delta C(t) = Q_{H,\,u} r_{ah,\,u} - Q_{H,\,r} r_{ah,\,r}$. Similarly, using Eqs. 13–14, the specific UDI effect can be written as a function of the BUHI intensity by adding and subtracting $\gamma_{q,u}{}' h_r$:

$$\Delta q(t) = \frac{\gamma_{q,u}{}'(1+2\beta)}{\gamma_\theta(1+\beta)}\Delta\theta(t) + \Delta\gamma_q{}' \cdot h_r(t), \tag{20}$$

or, alternatively, as a function of the CUHI:

$$\Delta q(t) = \frac{\gamma_{q,u}{}'(1+2\beta)}{\gamma_\theta(1+\beta)}\left[\Delta\theta_{2m}(t) - \frac{\Delta C_{2m}(t)}{\rho c_p}\right] + \Delta\gamma_q{}' \cdot h_r(t), \tag{21}$$

where $\Delta\gamma_q{}' = \gamma_{q,u}{}' - \gamma_{q,r}{}'$ and $\Delta C_{2m}(t) = Q_{H,\,2m,\,u} r_{ah,\,u} - Q_{H,\,2m,\,r} r_{ah,\,r}$. Eqs. 20–21 reveal that the BUHI-SUHI and UDI-CUHI relations are nonlinear due to the factors ΔC and $\Delta\gamma_q{}'$ which introduce an hysteresis effect. For further details, see the additional results provided in Supplementary Information (SI).

2.1.5. Cloud formation

The LCL height (LCL) can be estimated from θ and q as follows (Stull, 1988):

$$LCL(t) = \frac{R \cdot \theta(t)}{gM_a} \cdot ln\left[\frac{P_s}{P_{LCL}(t)}\right], \tag{22}$$

where $R = 8.314$ [J mol^{-1} K^{-1}] is the universal gas constant, g is the gravitational acceleration [ms^{-2}], $M_a = 29$ [g mol^{-1}] is the

molecular weight of air, P_s [kPa] is the atmospheric pressure at the canopy surface and P_{LCL} [kPa] is the atmospheric pressure at height $z = LCL$, which is given by Stull (1988):

$$P_{LCL}(t) = P_s\left[\frac{\theta_{LCL}(t)}{\theta(t)}\right]^{3.5}, \tag{23}$$

where θ_{LCL} [K] is the saturation temperature (dew point temperature) at the LCL height derived from the Clausius-Clapeyron equation, which is given by Stull (1988) as:

$$\theta_{LCL}(t) = \frac{2840}{3.5ln[\theta(t)\,] - ln\left[\frac{r(t)P_s}{0.622+r(t)}\right] - 7.108} + 55, \tag{24}$$

$r(t) \sim q(t)$ being the atmospheric water vapor mixing ratio, approximated by the specific humidity q as defined in Eq. 14.

As discussed earlier, convective cloud formation is defined by the crossing between the ABL and LCL height. Hence, we introduce the following function (Manoli et al., 2016):

$$\delta(t) = h(t) - LCL(t), \tag{25}$$

that defines a criterion for convective cloud formation. When δ=0, the ABL and LCL cross, so that a positive value of δ at the end of the day indicates that cloud formation has occurred at the ABL top, whereas clear sky conditions occur when δ remains negative. Even if, for shallow cumulus, it sometimes happens that the spatial mean LCL is still higher than the atmospheric boundary layer, the threshold δ=0 provides a simple and general criterion for convective cloud formation.

To further explore the impact of surface conditions on cloud formation, we estimate the time of crossing tc which indicates the time of day when h and LCL cross (i.e. $\delta(t = tc) = 0$, and the cloud base height, defined as the ABL height at time $t = tc$, i.e. $h(t_c)$. Note also that the crossing between the ABL and LCL heights is a necessary but not sufficient conditions for convective rainfall events (e.g. Juang et al., 2007; Manoli et al., 2016). Hence, even if we cannot predict rainfall triggering and quantify storm intensity, our simple framework provides a first order indication of possible urban-induced changes in the amount of precipitable water as rainfall depth is direclty linked to the atmospheric humidity profile (Konings et al., 2010) (see SI- Section 1.5).

2.2. Model set up

The surface energy balance of urban and rural areas is simulated using Eq.1 with different parameterisations for urban and rural areas (see Table 1). Following Christen and Vogt (2004), typical daytime values of the Bowen Ratio are approximated by a function of vegetation fraction:

$$Bo_u(f_v) = \frac{1}{f_v - f_v \cdot k_{Bo} + k_{Bo}} + Bo_r - 1, \tag{26}$$

where

$$k_{Bo} = \frac{1}{\left(Bo_{imp} - Bo_r + 1\right)}, \tag{27}$$

Bo_u is the average daytime Bowen Ratio for a given vegetation fraction f_v in the urban area, Bo_r is the known Bowen Ratio in the rural surroundings, and Bo_{imp} is a hypothetical Bowen Ratio for a completely impervious surface and k_{Bo} is a model parameter with value of 0.2 for the city of Basel (Christen and Vogt, 2004). The initial ABL height at sunrise can also be assumed to decrease linearly with the vegetation fraction (Theeuwes et al., 2015), i.e.

$$h_{0u}(f_v) = h_{0r} + (1 - f_v) \cdot h_{ref} \tag{28}$$

where h_{0u} is the initial urban boundary-layer height, h_{0r} is the initial rural ABL height (assumed to be known) and h_{ref} is a reference height. Based on field observations Theeuwes et al. (2015), the reference height is approximately 400 m. To simulate urban-rural changes in aerodynamic resistance (r_{ah}) [s m^{-1}] while keeping the model simple, we follow a similar procedure and assume that r_{ah} increases linearly with f_v, i.e.

$$r_{ah,u}(f_v) = r_{ah,r} + (1 - f_v) \cdot r_{ah,ref} \tag{29}$$

where $r_{ah,\,u}$ is the urban aerodynamic resistance, $r_{ah,\,r}$ is the rural aerodynamic resistance (assumed to be 66 [s m^{-1}] (Zhao et al., 2014)) and $r_{ah,\,ref}$ is a tuning parameter (assumed to be −16.33[s m^{-1}]) that ensures reasonable urban values (Zhao et al., 2014; Manoli et al., 2019). It should be noted that the aerodynamic resistance increases with vegetation fraction because of a rougher urban surface compared to the rural characteristics (Zhao et al., 2014). Hence, we are assuming that building height is constant and correlated with the level of imperviousness, which is a reasonable assumption in many cities (Zhang et al., 2022).

For the verification of the simulation results, we test the model against field observations (see next section). Subsequently, a sensitivity analysis is carried out to investigate how surface conditions (encoded in the vegetation fraction f_v) and free atmosphere states (encoded in the temperature and humidity lapse rates, γ_θ and γ_q) influence the three types of UHI intensities, as well as ABL

temperature, humidity, and the predisposition to convective cloud formation.

Specifically, we considered a gradient of imperviousness from fully vegetated/rural ($f_v = 1$) to entirely built environments ($f_v = 0$) and varied γ_θ and γ_q over a range of plausible values.

2.3. Study site

To test the model against field observations, we used measurements collected in The Basel Urban Boundary Layer Experiment (hereinafter BUBBLE Experiment) (Rotach et al., 2005), a year-long experiment investigating the boundary layer structure in the City of Basel, Switzerland.

In this study we selected data from four sites (two urban and two rural). At the urban sites, measurement towers were installed to measure turbulence at the height of at least twice the mean building height. The towers supported 6 ultrasonic anemometer-thermometers, full radiation components at tower top and inside the canyon, a temperature/humidity profile of 5 levels, 12 levels of cup anemometers and 10 levels with inlets for the CO_2/H_2O-analyzer. Data cover an intensive observation period of one month (from June to July 2002), but we selected only 8 fair-weather days when measurements of turbulent heat fluxes, air temperature, relative humidity, and ABL height were available (see SI). Given the objective of simulating typical clear sky conditions, observations were aggregated into average diurnal trends for urban and rural areas, respectively. The selected urban sites are Basel-Sperrstrasse (47.56 N;7.59E, 14.6 m average building height a.g.l) with $f_v = 0.16$ and Basel-Spalenring (47.55 N;7.57E, 12.5 m average building height a.g.l) with $f_v = 0.32$ while the rural sites are Grenzach (47.53 N; 8.67E) with $f_v = 0.91$ and Basel-Lange Erlen (47.59 N;7.64E) with $f_v = 0.94$. Further site and measurements details can be found elsewhere (e.g. Rotach et al., 2005; Christen et al., 2007). The time resolution of observations varies among different variables. Specifically, energy fluxes (H, LE, Q_S) and Mixed Layer height were averaged every 60 min, while Q^*, air and absolute temperature, as well as absolute and relative humidity were recorded every 10 min (Rotach et al., 2005). The height of the measurement also varies among different sites and variables. Specifically, urban relative humidity and air temperature were measured at 2.5 m and 25.5 m for Basel-Sperrstrasse and 3 m and 33 m for Basel-Spalenring. For the rural area, the two parameters were measured at 1.5 m for Grenzach and 2 m for Basel-Lange Erlen. It should be noted that the mixed layer height is estimated from observations using the Aerosol Mixed Layer height (AML height) obtained from the lidar signal during the BUBBLE Experiment. The model uses a temperature-based definition of the mixed layer and, even if the AML height is not exactly the same as the height of the ABL (Kotthaus et al., 2018), it can be considered as a good proxy for evaluation purposes (Rotach et al., 2005).

Note also that we tested the model using clear sky data to avoid any confounding effect as the model can simulate the ABL-LCL crossing but does not account for clouds' feedbacks (e.g. on radiation). While it would be interesting to compare the simulated timing of cloud formation with observations, it is not straightforward to causally link cloud observations to local scale convection activity. It is also difficult to clearly identify afternoon clouds in the observational data employed here (i.e. from June 10 to July 10, 2002), either because cloudiness persists from the early morning, because of data gaps, or because wind speed is high, thus making it

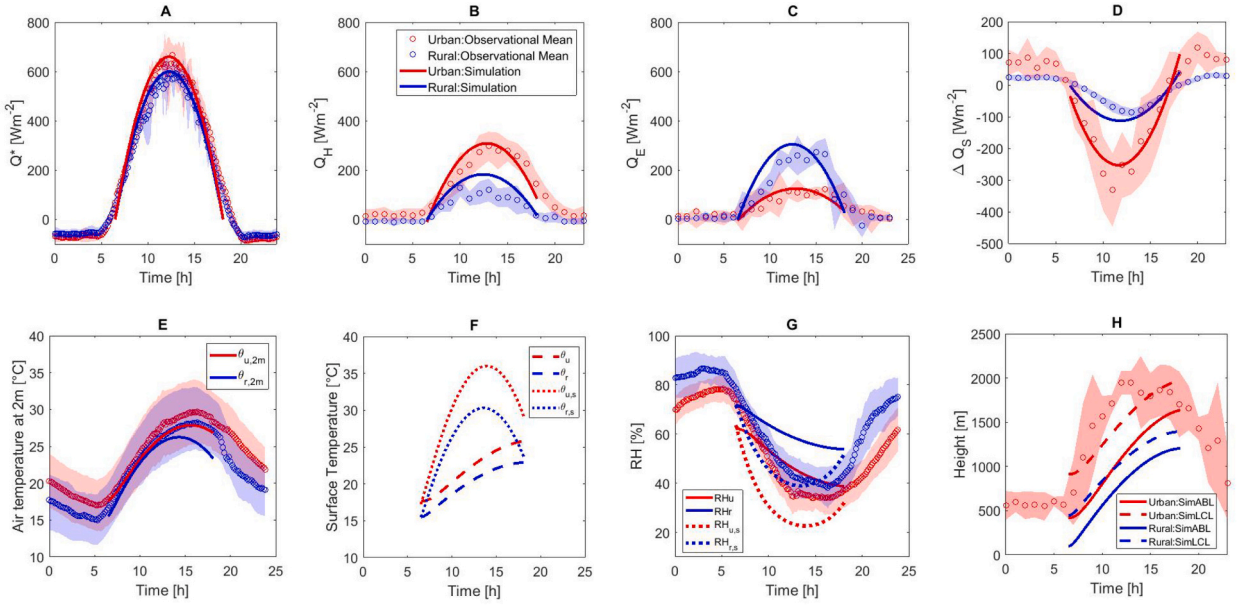

Fig. 2. Modelled and observed diurnal cycles of: (A) net radiation Q^*, (B) sensible heat flux Q_H, (C) latent heat flux Q_E, (D) storage heat flux ΔQ_S, (E) Air temperature at 2 m, (F) Surface Temperature θ_s and ABL temperature θ, (G) surface and ABL Relative Humidity (RH_s, RH), (H) ABL and LCL height. Symbols and shaded areas represent the mean of the observations from 8 fair-weather days ± 1 standard deviation. Note also that the heat storage flux was not measured at the urban sites and is shown here as residual of the energy balance.

difficult to distinguish convective events from regional circulation (see SI). For the sake of completeness, we have tested the model using observations from non-clear sky days presented elsewhere (results in the SI) but a proper observational assessment of convection triggering during summer afternoons is left for future work.

3. Results

3.1. Model testing

Simulation results are compared with the observations in Fig. 2, where the diurnal cycles of net radiation Q^* (Fig. 2A), sensible heat Q_H (Fig. 2B), latent heat Q_E (Fig. 2C), and storage heat flux ΔQ_S (Fig. 2D) are illustrated. Simulation results capture the timing and magnitude of the energy fluxes, both for urban and rural areas, with peak values observed between 12:00–14:00. The urban surface is characterized by a higher Bowen Ratio, leading to higher Q_H and lower Q_E fluxes (Fig. 2B). Imperviousness also contribute to a higher value of ΔQ_S (Fig. 2D). On the contrary, the higher vegetation cover of rural areas increases Q_E and decreases Q_H, thus causing a lower *Bo* (Fig. 2C). Overall, despite its simplicity, the model is shown to simulate the diurnal evolution of surface energy fluxes with reasonable accuracy.

The modelled diurnal 2-m air temperature and surface temperature are increasing from 08:30 until 14:00 (Fig. 2E and F). The maximum 2-m air temperature reaches 30 °C (Fig. 2E) while the surface temperature in the urban area rises to 37 °C (Fig. 2F). This leads to a significant surface and air temperature differences between urban and rural areas (Fig. 3A and B) because the sensible heat flux at the urban sites (Daily Max: 380 [W m^{-2}]) is larger than the rural ones (Daily Max: 200 [W m^{-2}]) as shown in Fig. 2B. When air and surface temperatures are increasing (08:30 to 14:00), the modelled relative humidity drops approximately by 25% while the observational data shows approximately a 50% drop for the same period (Fig. 2G). This discrepancy is attributable to the model simplifications but mainly to the height of the *RH* measurements which is not strictly representative of the simulated mixed layer humidity *q*. The modelled relative humidity in the rural area is higher than the urban area because a lower Bowen Ratio generates a higher Q_E as shown in Fig. 2C.

As for the growth of ABL and LCL, the simulated heights are fairly correct but there is a mismatch between the modelled and observed temporal trends. In particular, data show a faster increase in *h* while model simulations show a steady increase which does not reach the observed peak height. In general, the initial ABL height in the urban area is always higher than the rural area (Fig. 2H) and is supported by a higher sensible heat flux than its rural counterpart. As a result, the ABL height in the urban area is higher than that in the rural surrounding. In Fig. 2H, urban and rural ABL and LCL start to grow from 08:30 as the sensible heat flux increases, (see Eq.5). The modelled results here show no ABL-LCL crossing in the urban and rural area, which is consistent with the fact that data were collected during clear sky days.

Regarding the simulated UHI intensities, the initial CUHI (at 06:00) of 2°C decreases to 0.5 °C in the early morning and then starts to increase steadily after 10:00 up to a maximum value of 3.2°C in the evening (20:00) (see Fig. 3B). The BUHI follows a similar pattern, decreasing to 1.7°C in the early morning and increasing to approximate 3°C in the evening. These results are consistent with observations and show that BUHI and CUHI develop to their maximum value in the evening whereas the SUHI reaches its maximum value (5.7°C) during daytime. This is consistent also with evidence from the literature showing that maximum and minimum SUHI intensities typically occurs during daytime and nighttime, respectively (Chang et al., 2021), while the opposite is true for the CUHI (Oke et al., 2017; Venter et al., 2021). Note, however, that peak values of CUHI and BUHI occur after sunset but the model cannot reproduce such maxima as it is limited to daytime conditions only.

In terms of magnitude, our results shows that the SUHI is around 3°C higher than the CUHI during the day. This is in qualitative

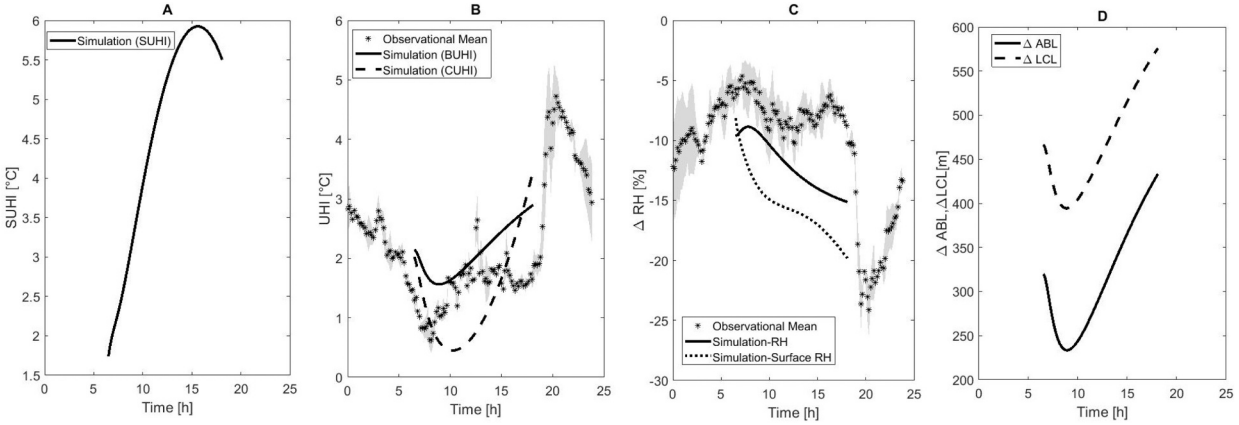

Fig. 3. Modelled and observed urban-rural differences: (A) $\Delta\theta_s$ (SUHI); (B) $\Delta\theta_{2m}$ (CUHI, black dotted line), $\Delta\theta$ (BUHI, black solid line) and the observations over 8 fair-weather days (asterisks); (C) ΔRH (black solid line) and ΔRH_s (black dotted line), (D) ΔABL (black solid line) and ΔLCL black dotted line).

agreement with the results by Du et al. (2021) showing that the annual mean daytime intensity of SUHIs in 366 global cities is greater than their CUHIs by 1.1 ± 1.9 ˚C (mean ± standard deviation), albeit some possible overestimation in our results. Furthermore, the simulated day-night difference of SUHI and CUHI (Fig. 3A,B) approaches positive and negative values respectively. Similar findings by Du et al. (2021) also suggest that the annual mean day–night difference in SUHI is generally positive (i.e., 0.6 ± 1.8 ˚C, while such a difference in CUHI becomes negative (i.e., −0.2 ± 1.6 ˚C). In terms of the urban-rural difference in ABL and LCL height, the simulated diurnal evolution of the urban-rural difference in LCL height shows a decrease from 450 m to 400 m in the early morning (06:00–09:00) and an sharp increase from 400 m to 550 m in the afternoon (10:00 to 17:00) (see Fig. 3D - dotted line). Urban-rural difference in ABL height shows a similar pattern (see Fig. 3D - solid line), decreasing to 230 m in the early morning (06:00–09:00) and increasing to approximate 425 m in the early evening (17:00). Both simulated results show that maximum urban-rural difference in ABL height occurs in the evening. This is in line with observations from Theeuwes et al. (2019) where urban-rural differences in sensible heat of approximately 50 W/m^2 are associated with a 1000 m increase in ABL height at around 6 pm.

3.2. Sensitivity analysis

Here we present the sensitivity analysis of the model to variations in f_v and γ_θ first and then f_v and γ_q. To ensure consistency with the model calibration, when varying γ_q the value of the potential temperature lapse rate is kept equal to 0.0078 [K m^{-1}] (i.e. the observed average over the 8 fair-weather days (Theeuwes et al., 2015)) but additional results are presented in the SI. In this sensitivity analysis, the vegetation fraction refers to the urban land cover which is varied from f_v=0 (fully urbanized) to 1 (fully vegetated), whereas the rural case is by definition always considered to be 1. The values observed at the urban and rural sites in Basel are are also illustrated for reference (e.g. symbols in Fig. 4). Note that for $f_v = 1$, some variables, such as the UHI intensities and ΔRH, are not zero as other factors contribute to urban warming/drying (i.e. changes in net radiation, anthropogenic heat, roughness) (Fig. 7A and B).

3.2.1. Potential temperature lapse rate and vegetation fraction

Regarding the impact of the potential temperature lapse rate on the BUHI, results show that, for the selected range of γ_θ, the maximum BUHI at $f_v = 0$ increases from 1˚C to 6˚C as illustrated in Fig. 4A. When considering the CUHI and SUHI, result show that the increase of lapse rate of potential temperature at $f_v = 0$ will have a maximum effect of 5˚C on CUHI (from 2˚C to 7˚C) and SUHI (from 5˚C to 10˚C) respectively. As expected, for a fixed value of potential temperature lapse rate, the UHI effect intensifies when the vegetation fraction of a city decreases. The maximum SUHI magnitude shows a sharper increase of 10˚C (from 0 to 10˚C) compared to 7˚C in CUHI (from 0 to 7˚C) and 6˚C in BUHI (from 0 to 6˚C) when vegetation fraction decreases (from 1 to 0). In short, low urban vegetation fractions and high potential temperature lapse rates lead to a higher magnitude of UHIs.

In terms of ΔRH between urban and rural sites, the increase of γ_θ will lead to a more considerable ΔRH (−25%) when the f_v approaches to zero, as shown in Fig. 5A. However, increasing the urban vegetation cover will create the expected reduction in ΔRH, until the same level of RH in urban and rural areas is achieved.

Regarding cloud formation, our result shows that the ABL starts crossing the LCL when the potential temperature lapse rate is lower than 0.008 [K m^{-1}] (Fig. 5B), which is close to the observed value of 0.0078 [K m^{-1}]. For larger values, cloudless condition (blue) occur regardless of the value of vegetation fraction of a city (Fig. 5B). For the selected sites and days, our simulations show little difference between urban (circle) and rural areas (triangle) when it comes to their predisposition to cloud formation. As a result, Fig. (5B) reveals that cloud formation is mostly affected by the free atmosphere lapse rates and there is a limited range of conditions ($0.006 < \gamma_\theta < 0.0065$ [K m^{-1}]) when changes in vegetation fraction can alter the cloud/cloudless regime.

Concerning the time of crossing (*tc*) between the ABL and LCL, the results show that *tc* is either zero (i.e. no crossing) or it can occur

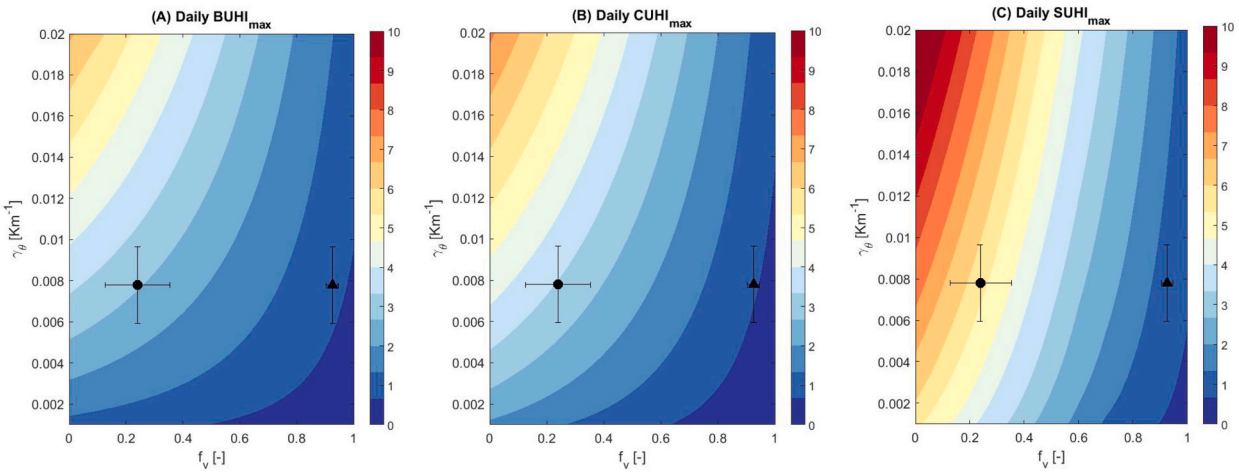

Fig. 4. Sensitivity Analysis of f_v and γ_θ: daily maximum of (A) BUHI [˚C]; (B) CUHI [˚C]; (C) SUHI [˚C]. Symbols and error bars represent the mean observational data with interquartile ranges for urban and rural sites, i.e. f_v=0.24 (Circle) and 0.93 (Triangle) respectively.

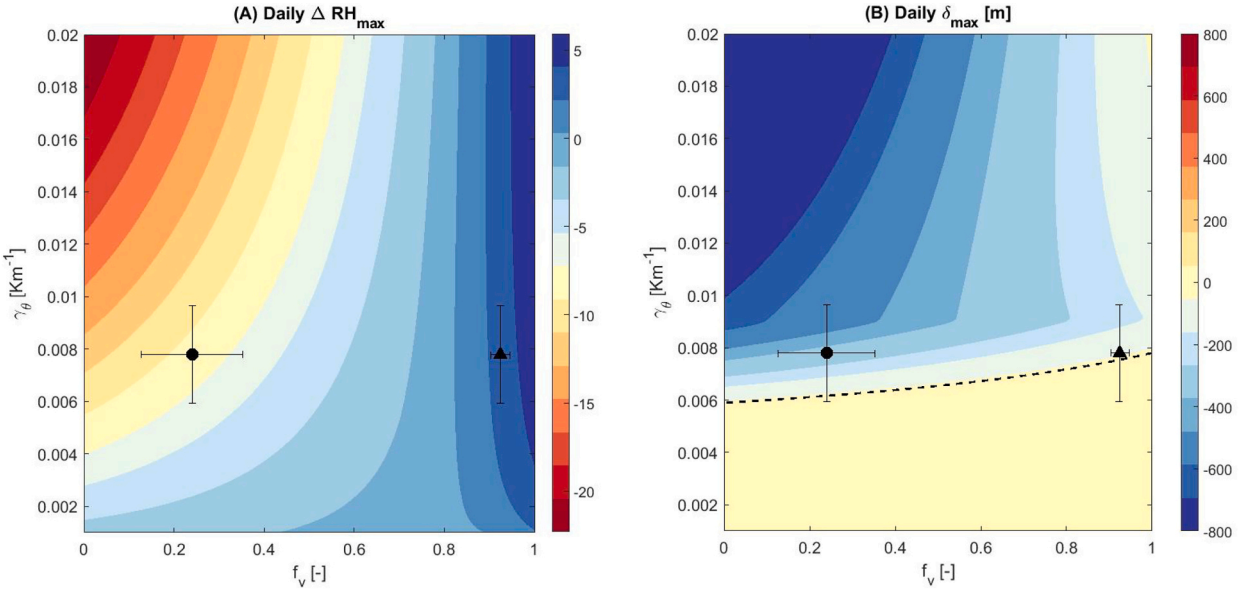

Fig. 5. Sensitivity Analysis to f_v and γ_θ of (A) daily maximum ΔRH[%]; (B) ABL-LCL Crossing [m], defined by $\delta_{max} = \delta(2t_0)$. The dotted black line is expressed by $\delta_{max} = 0$, representing the transition between two zones, $\delta_{max} > 0$ for cloud formation (yellow/red), $\delta_{max} < 0$ for cloudless conditions (light to dark blue); symbols and error bars represent the mean observational data with interquartile ranges for urban and rural sites, i.e. f_v=0.24 (Circle) and 0.93 (Triangle) respectively. (For interpretation of the references to colour in this figure legend, the reader is referred to the web version of this article.)

between 10 am and 5 pm for both cities and rural areas (Fig. 6A) with *tc* being slightly delayed with increasing imperviousness. These results also show that cities with less vegetation fraction generally have a higher value of ABL-LCL crossing height (1200-2000 m) as opposed to rural areas and cities with high vegetation fraction (800-1400 m) (Fig. 6B). This implies that convective cloud over urban areas can form at a higher height compared to rural regions.

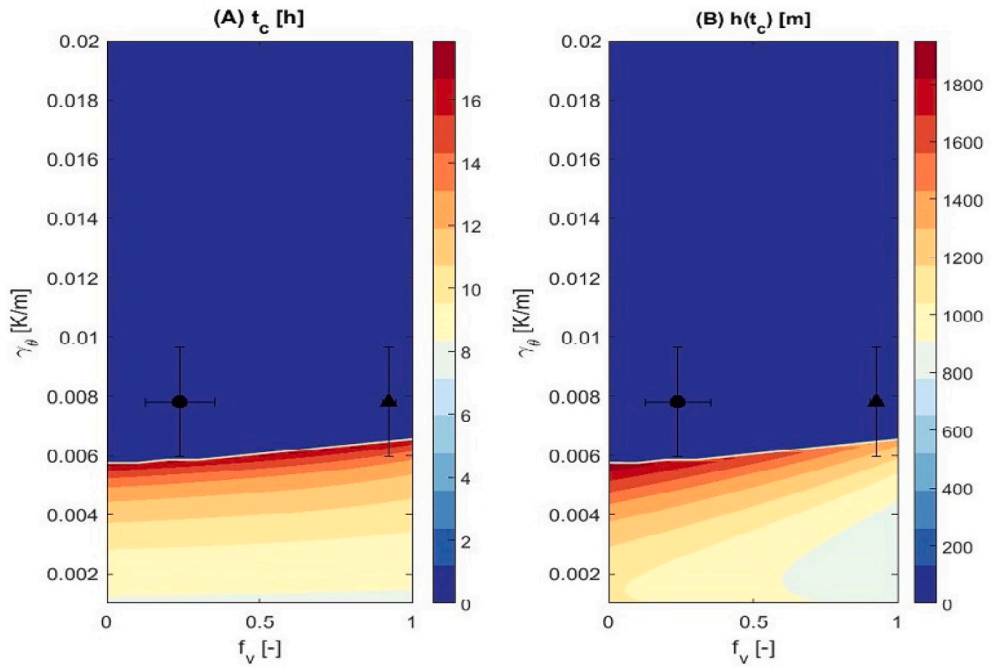

Fig. 6. Sensitivity Analysis to f_v and γ_θ of (A) time of crossing between ABL and LCL (t_c); (B) ABL height h at t_c. Symbols and error bars represent the mean observational data with interquartile ranges for urban and rural sites.

3.2.2. Specific humidity lapse rate and vegetation fraction

Figure 7A shows the correlation between the maximum daily value of UHI intensities and f_v. Since the UHI intensity does not depend on γ_q (see Eq.13), results are plotted as function of f_v only. As expected, the simulations show that less urban vegetation cover will lead to larger BUHI, CUHI and SUHI intensities (Fig. 7A) but, interestingly, a similar linear trend is observed for the three types of UHI intensities. However, the three types of UHIs show different negative slopes, leading to different maximum UHI values, i.e. BUHI of 2.5˚C, CUHI of 4˚C and SUHI of 7˚C, when f_v is zero. It should be noted that these maximum UHI values occur at different times of the day for the different types of UHIs. For example, the maximum SUHI occurs at mid-day while the maximum BUHI occurs in the evening.

Regarding the UDI effect, the maximum value of ΔRH is sensitive to the lapse rate of specific humidity and to urban vegetation cover as shown in Fig. 7B. The results show that the maximum simulated UDI effect is −18% when the f_v approaches zero and the air above the ABL is very dry. Note that ΔRH does not become zero for fv = 1 as the SUHI intensity because urban-rural differences in ABL dynamics are controlled also by differences in radiation, anthropogenic heat and roughness.

As for the cloud formation, the conditions observed at the urban and rural sites (circle and triangle in Fig. 7C, respectively) fall into the cloudless zone, which is consistent with the model calibration for fair-weather conditions. These results confirm that the urban vegetation cover has no impact on the occurrence of the ABL-LCL crossings when using the observed value of $\gamma_\theta = 0.0078$ [K m^{-1}] (Fig. 7C). However, the ABL and LCL heights become closer when γ_q increases (from −7 to -1×10^{-6} [kg kg^{-1} m^{-1}]) due to the decrease in LCL height in response to the increase in γ_q. Additional results presented in the SI reveals that changes in γ_q can indeed trigger convection when the value of γ_θ is varied.

4. Discussion

4.1. Impact of vegetation on UHIs, UDI, and convective clouds

We investigated the impact of urban vegetation cover on the UHI effect by simulating urban rural changes in surface energy fluxes and boundary layer dynamics with a simple analytical model. Observational evidence suggests that the global average of hourly daytime SUHIs is 1.45˚C and CUHIs is 0.26˚C (considering cities with more than one million inhabitants) (Venter et al., 2021) and the SUHI intensity correlates negatively with urban-rural differences in vegetation cover (e.g Peng et al., 2012; Paschalis et al., 2021). For the continental USA, the largest urban-rural temperature differences were found for urban areas displacing forests (with SUHI intensities of 6.5 − 9˚C) followed by temperate grasslands (6.3˚C) (Imhoff et al., 2010). A strong negative linear relationship between land surface temperature and vegetation fraction was also observed in the city of Shanghai(Li et al., 2011), confirming that imperviousness is a major cause of surface warming and urban vegetation can help mitigating the SUHI effect during summertime (Manoli et al., 2019), especially through urban forests (Paschalis et al., 2021). The presented simulations identified the same trend, i.e., a negative linear relationship between SUHI and vegetation fraction and revealed that the maximum daily values of BUHI and CUHI also decrease linearly with the increasing percentage of urban green spaces (Fig. 7A). Results in Fig. 7A also suggest that the vegetative cover has a greater impact on mitigating the SUHI compared to the CUHI and BUHI. A similar conclusion has been drawn by Du et al.

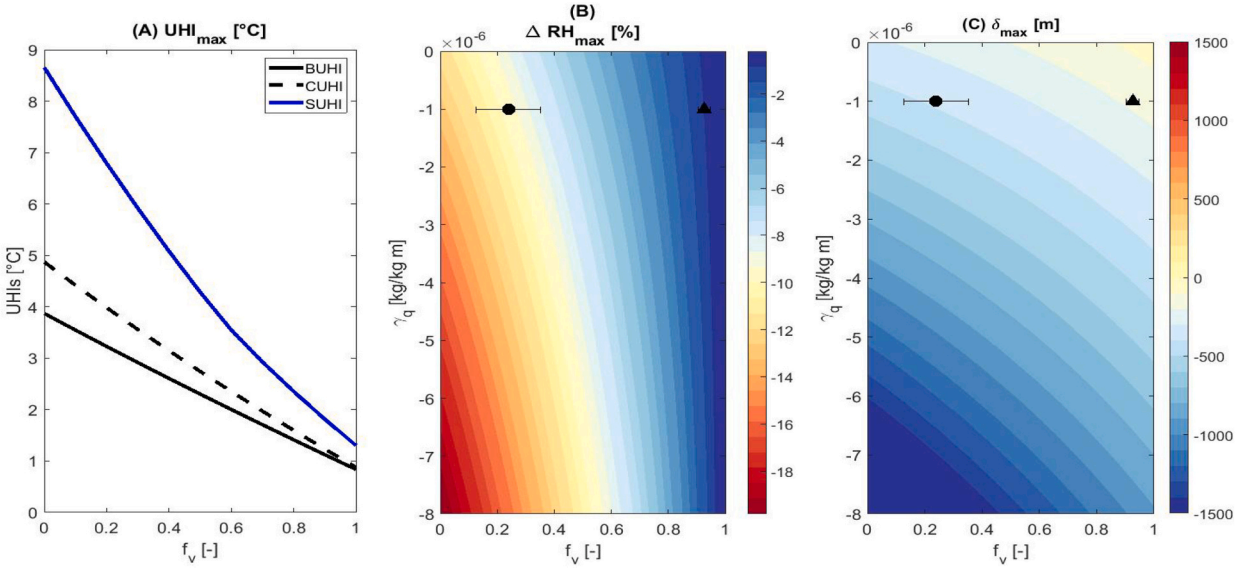

Fig. 7. Sensitivity analysis to f_v and γ_q of maximum (A) BUHI (black), CUHI (dotted black), SUHI (blue); (B) ΔRH; (C) $\delta_{max} = \delta(2t_0)$. The results here are obtained with $\gamma_\theta = 0.0078$ [K m^{-1}]. Symbols and error bars represent the mean observational data with interquartile ranges for urban and rural sites. (For interpretation of the references to colour in this figure legend, the reader is referred to the web version of this article.)

(2021) who showed that the difference in vegetation abundance exerts a greater impact on the SUHI than on the CUHI during the day. In general, the intensity of UHIs do not become zero for f_v=1 as urban warming is controlled by changes in evapotranspiration but also other factors such as radiation, anthropogenic heat and roughness (e.g Manoli et al., 2019; Meili et al., 2021).

With regards to cloud formation, some studies reported an increase in cloud cover over built up areas with respect to the rural surroundings (Romanov, 1999). This conclusion is supported by recent observational evidence of a systematic enhancement of afternoon cloud cover in the urban core of Paris and London during spring and summer (Theeuwes et al., 2019) which has been explained by urban-rural changes in surface heat release. Although our simulations also show an early release of storage heat flux from the urban site (as illustrated in Fig. 2D), the early release of storage heat flux is not sufficient enough to cause a higher growth rate of ABL height and no ABL-LCL crossing is therefore triggered (Fig. 2H). Hence, our simulations do not support an enhanced cloud formation due to surface heating, but attributing to other factors such as potential influence of the advective fluxes. This is consistent with other studies reporting a reduction in rainfall frequency over cities (Yang et al., 2021) and observations from forests and natural ecosystems (e.g. Manoli et al., 2016; Duveiller et al., 2021).

Our simulations suggest that, for the surface and FA conditions analysed in the model, urban areas are drier than the rural surroundings but there are not significant differences in the triggering of convective cloud formation, with a transition from cloudy to cloudless conditions largely controlled by the FA and occurring in the range $0.0065 < \gamma_\theta \leq 0.007$ [K m^{-1}] rather than by vegetation. The conditions observed at the study sites (symbols in Fig. 5B) show that cloud formation is slightly more likely in the rural area (closer to the transition threshold, dotted line in Fig. 5B) compared to the urban site.

The presented simulations also suggest that there is little difference between urban and rural sites in term of crossing occurrence, but the ABL-LCL crossing over cities occurs later in the day and at higher elevation, potentially causing more intense rainfall events (see results in the SI). Additional analyses presented in Fig. 8 in the SI show that the diurnal evolution of the LCL height is more sensitive to changes in vegetation fractions than the ABL height. Specifically, a reduction in vegetation fraction (and the associated change in UHI intensity, see Fig. 7A) will cause a larger increase in LCL than ABL height. Recent studies (Yang et al., 2021) also suggest that the LCL height rises over urban areas due to the effect of urban heat island, leading to a higher cloud base height. This is in line with our simulations and confirms the complex interplay between warming and drying. As a matter of fact, some studies show that urban areas decrease the frequency and intensity of light rainfall but increase the intensity and frequency of heavy rainfall (e.g. Zhang et al., 2018; Yan et al., 2020; Yang et al., 2021). Results here point in the same direction by showing that urban areas potentially experience higher cloud base height at a later time during the day compared to their rural counterparts, which is in line with the findings by Theeuwes

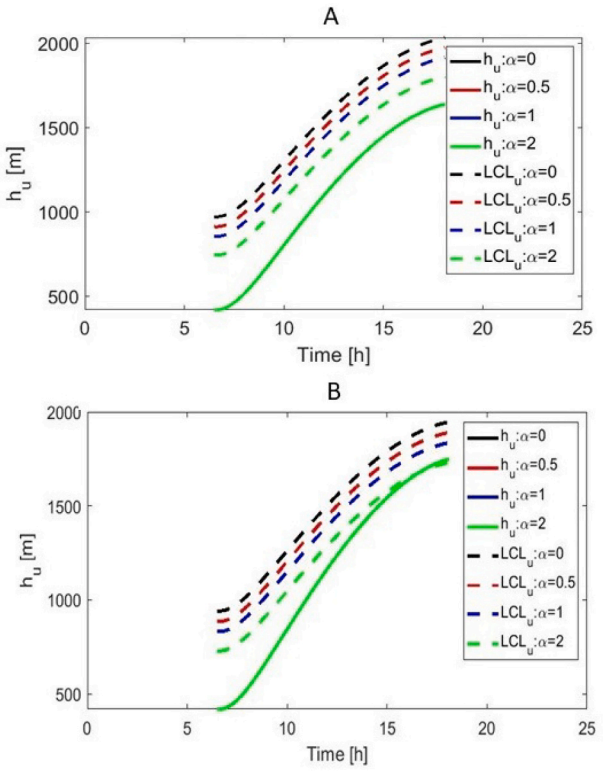

Fig. 8. Impact of moisture flux on ABL and LCL crossing. Modelled sensitivity of ABL (solid lines) and LCL Height (dashed lines) to α (black, red, blue and green colour represent α = 0,0.5,1,2 respectively), (A) modelled results by using $\gamma_\theta = 0.0078$ [K m^{-1}], (B) modelled results by using $\gamma_\theta = 0.0068$ [K m^{-1}]. It should be noted that the black, red and blue solid lines are overlapped by green solid line for both cases. (For interpretation of the references to colour in this figure legend, the reader is referred to the web version of this article.)

et al. (2019).

4.2. Advection of moisture

Our simple column model suggests that surface heat release is not necessarily the only cause for urban cloud formation. Differences between observation and our simple modeling results show the potential influence of additional factors, and advective fluxes in particular, may play a dominant role (e.g. Zhu et al., 2017; Lorenz et al., 2019; Lders and Olson, 2004; Yang et al., 2021). To assess the potential effect of lateral advection of moisture, we can include lateral moisture fluxes in the mass balance equation by re-writing the mositure budget in the well-mixed ABL as:

$$\rho h \frac{\partial q}{\partial t} = \frac{Q_E}{\lambda} + \rho\left(q_f - q\right)\frac{\partial h}{\partial t} + \Delta q, \tag{30}$$

For the sake of analytical tractability, we can assume Δq to be proportional to urban-rural changes in evapotranspiration, i.e. $\Delta q \sim \Delta f_v E_0$ where Δf_v is the urban-rural change in vegetation cover and E_0 is the actual evapotranspiration per unit area of vegetated surface (assumed equal in urban and rural areas) (Manoli et al., 2019, 2020a). Without loss of generality, we can therefore assume that Δq is proportional to urban evapotranspiration, i.e. $\Delta q = \alpha \frac{Q_E}{\lambda}$. Following the derivation in Section 2.1, the model can thus be modified to include moist advection by rewriting $\gamma_q^{'}$ as follow:

$$\gamma_q^{'} = \frac{1}{2}\left[\gamma_\theta \frac{c_p(1+\alpha)}{\lambda(1+2\beta)Bo} + \gamma_q\right]. \tag{31}$$

where α denotes the fraction of advected moisture relative to surface evaporation. The results in Fig. 8 show the impact of different values of α on the diurnal evolution of the LCL, demonstrating that the lateral advection of moist air can substantially influence the triggering of convection by lowering the LCL height and facilitating its crossing with the ABL. Moreover, the impact of different values of α on the ABL-LCL crossing becomes significant when the temperature lapse rate is slightly reduced (γ_θ from 0.0078 [K m^{-1}] in Panel A to 0.0068 [K m^{-1}] in Panel B). Hence, changes in α and γ_θ, can increase the chance of the occurrence of the ABL-LCL crossing. This supports the conclusion that moisture advection and atmospheric stability may play a key role in regulating cloud formation over urban areas (Theeuwes et al., 2022). Note, however, that the vertical profile of humidity and the moisture flux in the upper boundary layer can be major controls of cloud formation mechanisms (Theeuwes et al., 2022) but they cannot be properly resolved by the slab representation of the ABL employed here.

4.3. Limitations and perspectives

The slab model presented here provides novel insights into the relative importance of urban imperviousness and free atmosphere conditions on UHI, UDI and convection triggering. The approach is kept intentionally simple to assess whether the considered processes are primary controls of urban-rural differences in temperature, humidity, and cloud cover or not. Yet, given the objective of developing an analytical description of urban-rural dynamics, our approach has several limitations. The slab representation of the ABL neglects land-surface heterogeneities, which occurs over multiple scales, especially in urban contexts. Their inclusion in models remains a thorny problem in land-surface and atmospheric boundary-layer schemes for weather and climate forecasts. However, recent development in Large Eddy Simulations (LES) can help explore the effect of urban land surface heterogeneity and atmospheric dynamics on convective cloud formation (Wapler and Mayer, 2008; Theeuwes and Heus, 2010) and improve the parameterisation of simple slab models - such as the one proposed here. For the verification of the model, it should be noted that the presented model has only been tested with the Basel parameterisation, which represents a limited set of urban and climate characteristics. Hence, further work is needed to verify its applicability with other city charachteristics and local climatic zones. Also, given the objective of keeping the model simple, wind/drag effects and convergence/divergence of air were neglected. Here we employed a simple parameterisation for the aerodynamic resistances of urban and rural areas and we neglected near surface stability conditions and any possible alteration of the wind flow, which can potentially impact local climate and mesoscale circulations (Pielke and Avissar, 1990), with possible implication for convection triggering. Other factors, such as aerosol concentration and aerosol-cloud formation interaction, can also play a crucial role in determining urban-rural changes in cloud cover. Previous studies have summarised the potential causes of precipitation amplification over urban area, these being aerosol concentration, urban heat island, and changes in surface roughness (e.g. Thielen et al., 2000; Holst et al., 2016; Lu et al., 2019). In particular, aerosols can affect the energy balance of the earth-atmosphere system by direct scattering and absorption of radiation (e.g. Satheesh and Krishna Moorthy, 2005; Wright et al., 2010; Liu and Niyogi, 2019). How the atmospheric aerosols produced by the human activities in urban areas interact with cloud dynamics and the combined effect with other factors such as the UHI effect are important processes to consider in future studies.

5. Conclusion

In this study we presented an analytical model to quantify urban-rural changes in surface energy fluxes, boundary layer dynamics and the impact of urban areas/imperviousness on UHI intensities, UDIs and the triggering of convective clouds. We demonstrated that urban areas causes an increase in ABL and LCL heights due to higher Bowen Ratio compared to their rural surroundings. Our results show a strong effect of urban vegetation on the mitigation of all types of UHIs (i.e. BUHI, CUHI and SUHI). Considering the ABL-LCL

crossing over urban and rural surfaces as a criterion for cloudless and cloudy conditions, the simulations indicate that, for a range of free atmosphere conditions, an increase in impervious surface can suppress the initiation of convective clouds. Little difference between urban and rural areas is observed in terms of ABL-LCL crossing, but cloud formation is simulated to happen later during the day (afternoon) and at a higher elevation in urban areas compared to their rural counterparts. The later and higher crossing height causes higher cloud base height. These results suggest that surface heat release is not necessarily the major cause of cloud intensification over cities and call for further observational and modeling studies on the impact of urban areas on convective cloud formation.

CRediT authorship contribution statement

Clinton T.F. Chiu: Methodology, Formal analysis, Writing – original draft, Visualization. **Kai Wang:** Writing – review & editing. **Athanasios Paschalis:** Writing – review & editing. **Tohid Erfani:** Writing – review & editing. **Nadav Peleg:** Writing – review & editing. **Simone Fatichi:** Writing – review & editing. **Natalie Theeuwes:** Data curation, Writing – review & editing. **Gabriele Manoli:** Conceptualization, Methodology, Writing – review & editing, Supervision, Funding acquisition.

Declaration of Competing Interest

The authors declare that they have no known competing financial interests or personal relationships that could have appeared to influence the work reported in this paper.

Acknowledgements

CK, KW, and GM acknowledge support by “The Branco Weiss Fellowship - Society in Science” administered by ETH Zurich. SF acknowledges the support of the Singapore Ministry of Education Academic Research Fund Tier 1 through the project”Bridging scales from below: The role of heterogeneities in the global water and carbon budgets”. NP acknowledges the support of the Swiss National Science Foundation (SNSF), Grant 194649 (“Rainfall and floods in future cities”). NT acknowledges funding from the NWO rubicon grant”Clouds above the City”. AP knowledges funding from NERC (NE/S003495/1) and the Horizon 2020 project HEART (Grant agreement 945105). We also thank Matthias Rotach and Andreas Christen for making the data of the BUBBLE campaign available.

Appendix A. Supplementary data

Supplementary data to this article can be found online at https://doi.org/10.1016/j.uclim.2022.101346.

References

Angevine, W.M., White, A.B., Senff, C.J., Trainer, M., Banta, R.M., Ayoub, M.A., 2003. Urban-rural contrasts in mixing height and cloudiness over Nashville in 1999: urban-rural mixing height and cloudiness. J. Geophys. Res.-Atmos. 108 (D3) n/a–n/a.
Arnfield, A., 2005. Two decades of urban climate research: a review of turbulence, exchanges of energy and water, and the urban heat island. Int. J. Climatol. 23 (1).
Betts, A.K., 2009. Land-surface-atmosphere coupling in observations and models: land-surface-atmosphere coupling. J. Adv. Model. Earth Syst. 1 (3) n/a–n/a.
Betts, A.K., Ball, J.H., Beljaars, A.C.M., Miller, M.J., Viterbo, P.A., 1996. The land surface-atmosphere interaction: a review based on observational and global modeling perspectives. J. Geophys. Res.-Atmos. 101 (D3), 7209–7225.
Bhowmick, M., Parker, D.J., 2018. Analytical solution to a thermodynamic model for the sensitivity of afternoon deep convective initiation to the surface bowen ratio. Q. J. R. Meteorol. Soc. 144 (716), 2216–2229.
Bonetti, S., Manoli, G., Domec, J., Putti, M., Marani, M., Katul, G.G., 2015. The influence of water table depth and the free atmospheric state on convective rainfall predisposition. Water Resour. Res. 51 (4), 2283–2297.
Bouyer, J., 2009. Modelling and Simulation of Urban Microclimates - Study of the Urban Planning Impact on the Buildings Energy Consumption. Université de Nantes, Theses.
Chang, Y., Xiao, J., Li, X., Frolking, S., Zhou, D., Schneider, A., Weng, Q., Yu, P., Wang, X., Li, X., Liu, S., Wu, Y., 2021. Exploring diurnal cycles of surface urban heat island intensity in Boston with land surface temperature data derived from GOES-R geostationary satellites. Sci. Total Environ. 763, 144224.
Christen, A., 2005. Atmospheric Turbulence and Surface Energy Exchange in Urban Environments. PhD thesis,. University of Basel.
Christen, A., Vogt, R., 2004. Energy and radiation balance of a central European city. Int. J. Climatol. 24 (11), 1395–1421.
Christen, A., van Gorsel, E., Vogt, R., 2007. Coherent structures in urban roughness sublayer turbulence. Int. J. Climatol. 27 (14), 1955–1968.
Driedonks, A.G.M., Tennekes, H., de Bilt, 1984. Entrainment effects in the well-mixed atmospheric boundary layer. Bound.-Layer Meteorol. 30, 75–105.
Du, H., Zhan, W., Liu, Z., Li, J., Li, L., Lai, J., Miao, S., Huang, F., Wang, C., Wang, C., Fu, H., Jiang, L., Hong, F., Jiang, S., 2021. Simultaneous investigation of surface and canopy urban heat islands over global cities. ISPRS J. Photogramm. Remote Sens. 181, 67–83.
Duveiller, G., Filipponi, F., Ceglar, A., Bojanowski, J., Alkama, R., Cescatti, A., 2021. Revealing the widespread potential of forests to increase low level cloud cover. Nat. Commun. 12 (1), 4337.
Ek, M., Mahrt, L., 1994. Daytime evolution of relative humidity at the boundary layer top. Mon. Weather Rev. 122 (12).
Ek, M.B., Holtslag, A.A.M., 2004. Influence of soil moisture on boundary layer cloud development. J. Hydrometeorol. 5, 15.
Findell, K.L., Eltahir, E.A.B., 2003. Atmospheric controls on soil moisture–boundary layer interactions. Part I: framework development. J. Hydrometeorol. 4, 18.
Fortuniak, K., Christine Susan, B.G., Brian, O., 2005. Application of a slab surface energy balance model to determine surface parameters for urban areas. Lund eRep. Phys. Geog. 5, 90–91.
Garcia-Carreras, L., Parker, D.J., Marsham, J.H., 2011. What is the mechanism for the modification of convective cloud distributions by land surface–induced flows? J. Atmos. Sci. 68 (3), 619–634.
Garratt, J., 1993. The atmospheric boundary layer. J.R. Garrett, 1992. Hardbound. Cambridge University Press, 316 pp. Price: £50./ US $79.95. ISBN 0-521-38052-9. Earth-Sci. Rev. 34, 283–284.

Gentine, P., Ferguson, C.R., Holtslag, A.A.M., 2013a. Diagnosing evaporative fraction over land from boundary-layer clouds. J. Geophys. Res.-Atmos. 118 (15), 8185–8196.
Gentine, P., Holtslag, A.A., D'Andrea, F., Ek, M., 2013b. Surface and atmospheric controls on the onset of moist convection over land. J. Hydrometeorol. 14 (5), 1443–1462.
Grimmond, C., Cleugh, H., Oke, T., 1991. An objective urban heat storage model and its comparison with other schemes. Atmos. Environ. Part B. Urban Atmos. 25 (3).
Grimmond, C.S.B., Oke, T.R., 1999. Heat storage in urban areas: local-scale observations and evaluation of a simple model. J. Appl. Meteorol. 38, 19.
Grimmond, C.S.B., Blackett, M., Best, M.J., Barlow, J., Baik, J.-J., Belcher, S.E., Bohnenstengel, S.I., Calmet, I., Chen, F., Dandou, A., Fortuniak, K., Gouvea, M.L., Hamdi, R., Hendry, M., Kawai, T., Kawamoto, Y., Kondo, H., Krayenhoff, E.S., Lee, S.-H., Loridan, T., Martilli, A., Masson, V., Miao, S., Oleson, K., Pigeon, G., Porson, A., Ryu, Y.-H., Salamanca, F., Shashua-Bar, L., Steeneveld, G.-J., Tombrou, M., Voogt, J., Young, D., Zhang, N., 2010. The international urban energy balance models comparison project: first results from phase 1. J. Appl. Meteorol. Climatol. 49 (6), 1268–1292.
Grimmond, C.S.B., Ward, H., Kotthaus, S. (Eds.), 2015. How Is Urbanization Altering Local and Regional Climate?, 1 edition edition. Routledge, Taylor & Francis Group, London; New York.
Grimmond, S., 2007. Urbanization and global environmental change: local effects of urban warming. Geogr. J. 173 (1), 83–88.
Haiden, T., 1997. An analytical study of cumulus onset. Q. J. R. Meteorol. Soc. 123 (543), 1945–1960.
Hao, L., Huang, X., Qin, M., Liu, Y., Li, W., Sun, G., 2018. Ecohydrological processes explain urban dry island effects in a wet region, Southern China. Water Resour. Res. 54 (9), 6757–6771.
Holst, C.C., Tam, C.-Y., Chan, J.C.L., 2016. Sensitivity of URBAN rainfall to anthropogenic heat flux: a numerical experiment: sensitivity of urban rainfall to ah. Geophys. Res. Lett. 43 (5), 2240–2248.
Howard, L., 1833. The Climate of London: Deduced from Meteorological Observations Made in the Metropolis and at Various Places Around it. Harvey and Darton, J. and A. Arch, Longman, Hatchard, S. Highley [and] R. Hunter, 3, p. 453.
Huang, J., Fatichi, S., Mascaro, G., Manoli, G., Peleg, N., 2022. Intensification of sub-daily rainfall extremes in a low-rise urban area. Urban Clim. 42, 101124.
Imhoff, M.L., Zhang, P., Wolfe, R.E., Bounoua, L., 2010. Remote sensing of the urban heat island effect across biomes in the continental USA. Remote Sens. Environ. 114 (3), 504–513.
Juang, J.-Y., Porporato, A., Stoy, P.C., Siqueira, M.S., Oishi, A.C., Detto, M., Kim, H.-S., Katul, G.G., 2007. Hydrologic and atmospheric controls on initiation of convective precipitation events: hydrologic and atmospheric controls. Water Resour. Res. 43 (3).
Konings, A.G., Katul, G.G., Porporato, A., 2010. The rainfall-no rainfall transition in a coupled land-convective atmosphere system: rainfall-no rainfall transition. Geophys. Res. Lett. 37 (14), L14401.
Kotthaus, S., Halios, C.H., Barlow, J.F., Grimmond, C., 2018. Volume for pollution dispersion: London's atmospheric boundary layer during ClearfLo observed with two ground-based lidar types. Atmos. Environ. 190, 401–414.
Kusaka, H., Kondo, H., Kikegawa, Y., Kimura, F., 2001. A simple single-layer urban canopy model for atmospheric models: comparison with multi-layer and slab models. Bound.-Layer Meteorol. 101 (3), 329–358.
Lders, N.M., Olson, M.A., 2004. Impact of urban effects on precipitation in high latitudes. M O 5, 21.
Li, D., Liao, W., Rigden, A.J., Liu, X., Wang, D., Malyshev, S., Shevliakova, E., 2019. Urban heat island: aerodynamics or imperviousness? Sci. Adv. 5 (4), eaau4299.
Li, J., Song, C., Cao, L., Zhu, F., Meng, X., Wu, J., 2011. Impacts of landscape structure on surface urban heat islands: a case study of Shanghai, China. Remote Sens. Environ. 115 (12), 3249–3263.
Liu, J., Niyogi, D., 2019. Meta-analysis of urbanization impact on rainfall modification. Sci. Rep. 9 (1), 7301.
Lorenz, J.M., Kronenberg, R., Bernhofer, C., Niyogi, D., 2019. Urban rainfall modification: observational climatology over Berlin, Germany. J. Geophys. Res.-Atmos. 124 (2), 731–746.
Lu, Jiang, Ren, Zhang, Wang, Liu, and Wei (2019). Spatial and temporal variability in precipitation concentration over mainland China, 1961–2017. Water, 11(5): 881.
Manoli, G., Domec, J.-C., Novick, K., Oishi, A.C., Noormets, A., Marani, M., Katul, G., 2016. Soil-plant-atmosphere conditions regulating convective cloud formation above southeastern US pine plantations. Glob. Chang. Biol. 22 (6), 2238–2254.
Manoli, G., Fatichi, S., Schläpfer, M., Yu, K., Crowther, T.W., Meili, N., Burlando, P., Katul, G.G., Bou-Zeid, E., 2019. Magnitude of urban heat islands largely explained by climate and population. Nature 573 (7772), 55–60.
Manoli, G., Fatichi, S., Bou-Zeid, E., Katul, G.G., 2020a. Seasonal hysteresis of surface urban heat islands. Proc. Natl. Acad. Sci. 117 (13), 7082–7089.
Manoli, G., Fatichi, S., Schläpfer, M., Yu, K., Crowther, T.W., Meili, N., Burlando, P., Katul, G., Zeid, E.B., 2020b. Reply to martilli et al.(2020): Summer Average Urban-rural Surface Temperature Differences do not Indicate the Need for Urban Heat Reduction.
Martilli, A., Roth, M., Chow, W.T., Demuzere, M., Lipson, M., Krayenhoff, E.S., Sailor, D., Nazarian, N., Voogt, J., Wouters, H., et al., 2020. Summer Average Urban-Rural Surface Temperature Differences Do Not Indicate the Need for Urban Heat Reduction.
Meili, N., Manoli, G., Burlando, P., Carmeliet, J., Chow, W.T., Coutts, A.M., Roth, M., Velasco, E., Vivoni, E.R., Fatichi, S., 2021. Tree effects on urban microclimate: diurnal, seasonal, and climatic temperature differences explained by separating radiation, evapotranspiration, and roughness effects. Urban For. Urban Green. 58, 126970.
Meili, N., Paschalis, A., Manoli, G., Fatichi, S., 2022. Diurnal and seasonal patterns of global urban dry islands. Environ. Res. Lett. 17 (5), 054044.
Oke, T., 1982. The energetic basis of the urban heat island. Q. J. R. Meteorol. Soc. 9 (12).
Oke, T.R., 1973. City Size and the Urban Heat Island, 7. Atmospheric Environment Pergamon Press, pp. 769–779.
Oke, T.R., Mills, G., Christen, A., Voogt, J.A., 2017. Urban Climates. Cambridge University Press, Cambridge.
Onomura, S., Grimmond, C., Lindberg, F., Holmer, B., Thorsson, S., 2015. Meteorological forcing data for urban outdoor thermal comfort models from a coupled convective boundary layer and surface energy balance scheme. Urban Clim. 11, 1–23.
Pal, S., Clark, N.E., Lee, T.R., Conder, M., Buban, M., 2021. When and where horizontal advection is critical to alter atmospheric boundary layer dynamics over land: the need for a conceptual framework. Atmos. Res. 264, 105825.
Paschalis, A., Chakraborty, T., Fatichi, S., Meili, N., Manoli, G., 2021. Urban forests as main regulator of the evaporative cooling effect in cities. AGU Adv. 2 (2).
Pataki, D.E., Carreiro, M.M., Cherrier, J., Grulke, N.E., Jennings, V., Pincetl, S., Pouyat, R.V., Whitlow, T.H., Zipperer, W.C., 2011. Coupling biogeochemical cycles in urban environments: ecosystem services, green solutions, and misconceptions. Front. Ecol. Environ. 9 (1), 27–36.
Peng, S., Piao, S., Ciais, P., Friedlingstein, P., Ottle, C., Bréon, F.-M., Nan, H., Zhou, L., Myneni, R.B., 2012. Surface urban heat Island across 419 global big cities. Environ. Sci. Technol. 46 (2), 696–703.
Pielke, R.A., 2001. Influence of the spatial distribution of vegetation and soils on the prediction of cumulus convective rainfall. Rev. Geophys. 39 (2), 151–177.
Pielke, R.A., Avissar, R., 1990. Influence of landscape structure on local and regional climate. Landsc. Ecol. 4 (2–3), 133–155.
Porporato, A., 2009. Atmospheric boundary-layer dynamics with constant bowen ratio. Bound.-Layer Meteorol. 132 (2).
Risser, M.D., Wehner, M.F., 2017. Attributable human-induced changes in the likelihood and magnitude of the observed extreme precipitation during hurricane harvey. Geophys. Res. Lett. 44 (24).
Romanov, P., 1999. Urban influence on cloud cover estimated from satellite data. Atmos. Environ. 33, 4163–4172.
Rotach, M.W., Vogt, R., Bernhofer, C., Batchvarova, E., Christen, A., Clappier, A., Feddersen, B., Gryning, S.-E., Martucci, G., Mayer, H., Mitev, V., Oke, T.R., Parlow, E., Richner, H., Roth, M., Roulet, Y.-A., Ruffieux, D., Salmond, J.A., Schatzmann, M., Voogt, J.A., 2005. BUBBLE – an urban boundary layer meteorology project. Theor. Appl. Climatol. 81 (3–4), 231–261.
Satheesh, S.K., Krishna Moorthy, K., 2005. Radiative effects of natural aerosols: a review. Atmos. Environ. 39 (11), 2089–2110.
Shepherd, M., 2005. A review of current investigations of urban-induced rainfall and recommendations for the future. Earth Interact. 9 (12).
Siqueira, M., Katul, G., Porporato, A., 2009. Soil moisture feedbacks on convection triggers: the role of soil–plant hydrodynamics. J. Hydrometeorol. 10 (1), 96–112.
Stevens, B., 2006. Bulk boundary-layer concepts for simplified models of tropical dynamics. Theor. Comput. Fluid Dyn. 20 (5–6), 279–304.
Stull, R. B. (1988). An Introduction to Boundary Layer Meteorology. Atmospheric sciences library. Kluwer Academic Publishers, Dordrecht; Boston.

Tennekes, H., 1973. A model for the dynamics of the inversion above a convective boundary layer. J. Atmos. Sci. 30 (4).
Theeuwes, N., Heus, T., 2010. The Influence of Radiation on Cloud-surface Feedback Mechanisms Using Large Eddy Simulation, p. 16.
Theeuwes, N.E., Steeneveld, G.-J., Ronda, R.J., Rotach, M.W., Holtslag, A.A.M., 2015. Cool city mornings by urban heat. Environ. Res. Lett. 10 (11), 114022.
Theeuwes, N.E., Steeneveld, G.-J., Ronda, R.J., Holtslag, A.A.M., 2017. A diagnostic equation for the daily maximum urban heat island effect for cities in northwestern Europe: diagnostic equation for the urban heat Island. Int. J. Climatol. 37 (1), 443–454.
Theeuwes, N.E., Barlow, J.F., Teuling, A.J., Grimmond, C.S.B., Kotthaus, S., 2019. Persistent cloud cover over mega-cities linked to surface heat release. NPJ Clim. Atmos. Science 2 (1), 15.
Theeuwes, N.E., Boutle, I.A., Clark, P.A., Grimmond, S., 2022. Understanding London's summertime cloud cover. Q. J. R. Meteorol. Soc. 148 (742), 454–465.
Thielen, J., Wobrock, W., Gadian, A., Mestayer, P.G., 2000. The Possible Influence of Urban Surfaces on Rainfall Development: A Sensitivity Study in 2D in the Meso-g-scale page 25.
UN-DESA, 2018. The 2018 Revision of World Urbanization Prospects. Technical Report. The Population Division, The Department of Economic and Social Affairs, the United Nations, New York.
Venter, Z.S., Chakraborty, T., Lee, X., 2021. Crowdsourced air temperatures contrast satellite measures of the urban heat island and its mechanisms. Sci. Adv. 7 (22), eabb9569.
Wapler, K., Mayer, B., 2008. A fast three-dimensional approximation for the calculation of surface irradiance in large-Eddy simulation models. J. Appl. Meteorol. Climatol. 47 (12), 3061–3071.
Ward, H., Kotthaus, S., Järvi, L., Grimmond, C., 2016. Surface urban energy and water balance scheme (SUEWS): development and evaluation at two UK sites. Urban Clim. 18, 1–32.
Wright, M.E., Atkinson, D.B., Ziemba, L., Griffin, R., Hiranuma, N., Brooks, S., Lefer, B., Flynn, J., Perna, R., Rappenglück, B., Luke, W., Kelley, P., 2010. Extensive aerosol optical properties and aerosol mass related measurements during TRAMP/TexAQS 2006 – implications for PM compliance and planning. Atmos. Environ. 44 (33), 4035–4044.
Yan, M., Chan, J.C.L., Zhao, K., 2020. Impacts of urbanization on the precipitation characteristics in Guangdong Province, China. Adv. Atmos. Sci. 37 (7), 696–706.
Yang, P., Ren, G., Yan, P., Deng, J., 2021. Urbanization reduces frequency of light rain: an example from Beijing City. Theor. Appl. Climatol. 145 (1), 763–774.
Yin, J., Albertson, J.D., Rigby, J.R., Porporato, A., 2015. Land and atmospheric controls on initiation and intensity of moist convection: cape dynamics and lcl crossings. Water Resour. Res. 51 (10), 8476–8493.
Zhang, W., Villarini, G., Vecchi, G.A., Smith, J.A., 2018. Urbanization exacerbated the rainfall and flooding caused by hurricane Harvey in Houston. Nature 563 (7731), 384–388.
Zhang, Z., Paschalis, A., Mijic, A., Meili, N., Manoli, G., van Reeuwijk, M., Fatichi, S., 2022. A mechanistic assessment of urban heat island intensities and drivers across climates. Urban Clim. 44, 101215.
Zhao, L., Lee, X., Smith, R.B., Oleson, K., 2014. Strong contributions of local background climate to urban heat islands. Nature 511 (7508), 216–219.
Zhu, X., Li, D., Zhou, W., Ni, G., Cong, Z., Sun, T., 2017. An idealized LES study of urban modification of moist convection: urban modification of moist convection. Q. J. R. Meteorol. Soc. 143 (709), 3228–3243.